Journal of Applied Electrochemistry (2005) 35:1087–1093
DOI 10.1007/s10800-005-9003-0

Electrochemical incineration of oxalic acid: Reactivity and engineering parameters

C.A. MARTÍNEZ-HUITLE, S. FERRO and A. DE BATTISTI*
Department of Chemistry, University of Ferrara, via L. Borsari 46, I-44100, Ferrara, Italy
*(*author for correspondence, fax: +39-0532-240709; e-mail: dbtcll@unife.it)*

Received 22 July 2004; accepted in revised form 7 June 2005

Key words: anode material, electrochemical incineration, flow cell, mass transfer coefficient, oxalic acid

Abstract

Mass transfer measurements were carried out to test a disk-shaped parallel-plate electrochemical cell, based on a new design. The impinging-jet-cell concept, confined between parallel plates, was adapted to a configuration with one central inlet and several peripheral exit sections, leading to more effective hydrodynamics within the cell. Measurements of mass transfer coefficient were performed using the limiting diffusion current technique based on ferro-cyanide ion oxidation, and overall mass transfer coefficients were correlated to Reynolds numbers ranging from 30 to 200.

A comparison with literature on similar devices showed higher mass transfer coefficients can be obtained in the cell described in the present work. From the mass transfer standpoint, this type of cell could be a valuable tool in electrochemical wastewater treatment applications.

The electrochemical oxidation of oxalic acid was tested at different anode materials (Pb/PbO_2, boron-doped diamond, Ti/Pt and Ti/IrO_2–Ta_2O_5), showing that the new cell design enables limitations usually encountered with conventional batch cells to be overcome. However, the nature of the anode material remains an important parameter for the elimination of organic substrates.

List of symbols

A	electrode surface area (m^2)
C	bulk species concentration (mol m^{-3})
D	diffusion coefficient (m^2 s^{-1})
d_N	diameter of the nozzle (m)
F	faradic constant (96487 C mol^{-1})
H	nozzle height (m)
I_L	electrolysis limiting current (A)
K	mass transfer coefficient (m s^{-1})
r	radial coordinate measured from the stagnation point (m)
R	radius of the disk electrode (cm)
Re	Reynolds number
Re_d	nozzle Reynolds number
Re_r	radial Reynolds number
s	inter-electrode distance (m)
Sc	Schmidt number
Sh	Sherwood number
Sh_d	nozzle Sherwood number
Sh_r	radial Sherwood number
z	electrons exchanged in electrode reaction
V_N	mean fluid velocity in cell or channel (m s^{-1})
Q	volumetric flow rate (m^3 s^{-1})

Greek letters

ρ	fluid density (kg m^{-3})
ν	kinematics viscosity of the fluid (m^2 s^{-1})
μ	dynamic viscosity (kg s^{-1} m^{-1})

1. Introduction

Many electrochemical processes are carried out under limiting or near limiting current conditions, in order to maximize the space-time yield of the electrolyser. As a result, mass transport determines the rate of conversion of reactants to products and it is common to use inert turbulence promoters, such as baffles and/or a high fluid velocity, to enhance the mass transport to or from the electrode surface and, hence, the cell current density [1]. Cells consisting of planar electrodes in a parallel plate configuration are among the most frequently used type of electrochemical reactor for industrial applications. Such reactors combine simplicity of design, manufacture and versatility, permitting their use in several processes. However, an increase in the mass transfer coefficient is often the result of a complex combination of geometry and hydrodynamics, especially in the inlet and outlet

sections of the cell. The relationship between cell flow conditions and the mass transfer performance, in parallel plate cell geometry, has recently been described for some specific cases [2]. Goodridge et al. [3] have studied mass transfer in baffled cells of different sizes, using the electrochemical limiting current measurement method. Wragg and Leontaritis [4] have described measurements of local mass transfer and current distribution in parallel plate cells of similar dimensions to those of Goodridge's cells. The mass transfer distributions near cell inlets and corners, in the case of a rectangular-shaped electrochemical flow cell [5], and the effects of baffle length on mass transfer [1] have also been investigated, while Bengoa et al. [6] have carried out flow visualization studies and modelling for a filter-press-type electrochemical reactor. Several studies have been realized [7–13] concerning the experimental conditions, phenomena, interactions, inert turbulence promoters, design of cells, as well as the mathematical modelling of processes, allowing important hydrodynamic improvements in the electrochemical processes under investigation. Moreover, different types of cells have been proposed in recent years; an efficient cell design has been obtained through the modification of specific electrode area and/or mass transport coefficient optimisation [14].

Highly effective surface convective transfer rates have been obtained through the use of a single impinging jet, or an array of such jets, as witnessed by a wide range of industrial and technological applications [15]. In these cases, a submerged circular jet of electrolyte impinges on a flat plate, normal to the direction of flow; the electrode is a circular disc embedded on the flat plate at the stagnation point [15, 16]. Industrial applications include both liquid and gaseous flows, for the annealing of metal and plastic sheets, tempering of glass plates, drying of textiles, paper, veneer and film materials, cooling of heated components in turbine engines, and de-icing of aircraft systems [17, 18].

In the field of wastewater treatments, and in addition to traditional heavy metal abatement [14], electrochemistry may find interesting applications in the context of organic incineration [13], offering both process versatility and reactor simplicity, in terms of construction and management. Additionally, electrochemical oxidation processes imply potential cost effectiveness and environmental compatibility for the degradation of different organic pollutants [19]. The electrochemical oxidation method has been proposed, in particular, for the destruction or conversion of mixed wastes containing refractory organic pollutants or toxic substances. The main purpose of the wastewater treatment is the complete oxidation of organics to CO_2 [20–23] or the conversion of toxics to biocompatible compounds [24, 25]. Several anodic materials have been investigated for the elimination of organic pollutants, including metal-oxide anodes such as IrO_2 [26, 27], PbO_2 [28–31], SnO_2 [23, 32] and SnO_2–Sb_2O_5 [33]. More recently, the list of possible candidates has been further enriched with the involvement of Ti/Diamond (Ti/BDD) [34] and Si/Diamond (Si/BDD) [35].

In this work, a detailed mass transfer characterization of an electrochemical cell with a new design will be initially presented; subsequently, results on the application of the cell to the electro-oxidation of oxalic acid (OA) will be discussed. The electro-oxidation investigation was performed using Ti/Pt, Si/BDD, Pb/PbO_2 and Ti/IrO_2–Ta_2O_5 electrodes. As reported in the literature, carboxylic acids are common intermediates in the oxidative degradation of several organic substrates; also, they are quite stable and their mineralization is quite elaborate. This seems to hold true, in particular, for OA, which is the last intermediate in a number of wastewater treatment processes [19]. Consequently, oxalic acid was selected as a model organic substrate in this research.

2. Experimental

2.1. *Cell and electrodes*

Figure 1 shows the flow cell with parallel disc plate electrodes; initially, the assembly was put together with a nickel anode and a Ti/Pt cathode, both 0.5 mm thick and with an active area of 63.5 cm^2; the inter-electrode gap was 10 mm. The cell had one inlet and several outlet sections, all positioned along its central element; compartments were made of PVC and constructed so as to accommodate the disc plate electrodes, as shown in Figure 2. The cell inlet (nozzle, d_N) was designed in such a way as to direct the solution at the centre of the anodic disk electrode, thus obtaining well distributed circulation of the fluid inside the cell, as described in Figure 1c. The diameter of the nozzle was 4.5 mm, as was the distance between the nozzle exit and the anode surface (H). The electrolyte was stored in a glass tank and circulated through the cell by means of a peristaltic pump, at a constant flow rate.

2.2. *Techniques and instrumentation*

Characterization of the flow cell was achieved using an equimolar aqueous solution of potassium ferro-cyanide and ferri-cyanide in NaOH. Both the partners of the redox couple were considered together, to ensure a constant composition for the electrolyte during the measurements; the physical properties of the test solution [4] are shown in Table 1.

The electrochemical reactions are the following:

$$Fe(CN)_6^{3-} + e \rightarrow Fe(CN)_6^{4-} \qquad \text{at the cathode}$$

$$Fe(CN)_6^{4-} \rightarrow Fe(CN)_6^{3-} + e \qquad \text{at the anode}$$

Mass transfer coefficients were determined through the well-known diffusion limiting current technique [5, 36], focusing on the oxidation reaction (limiting current

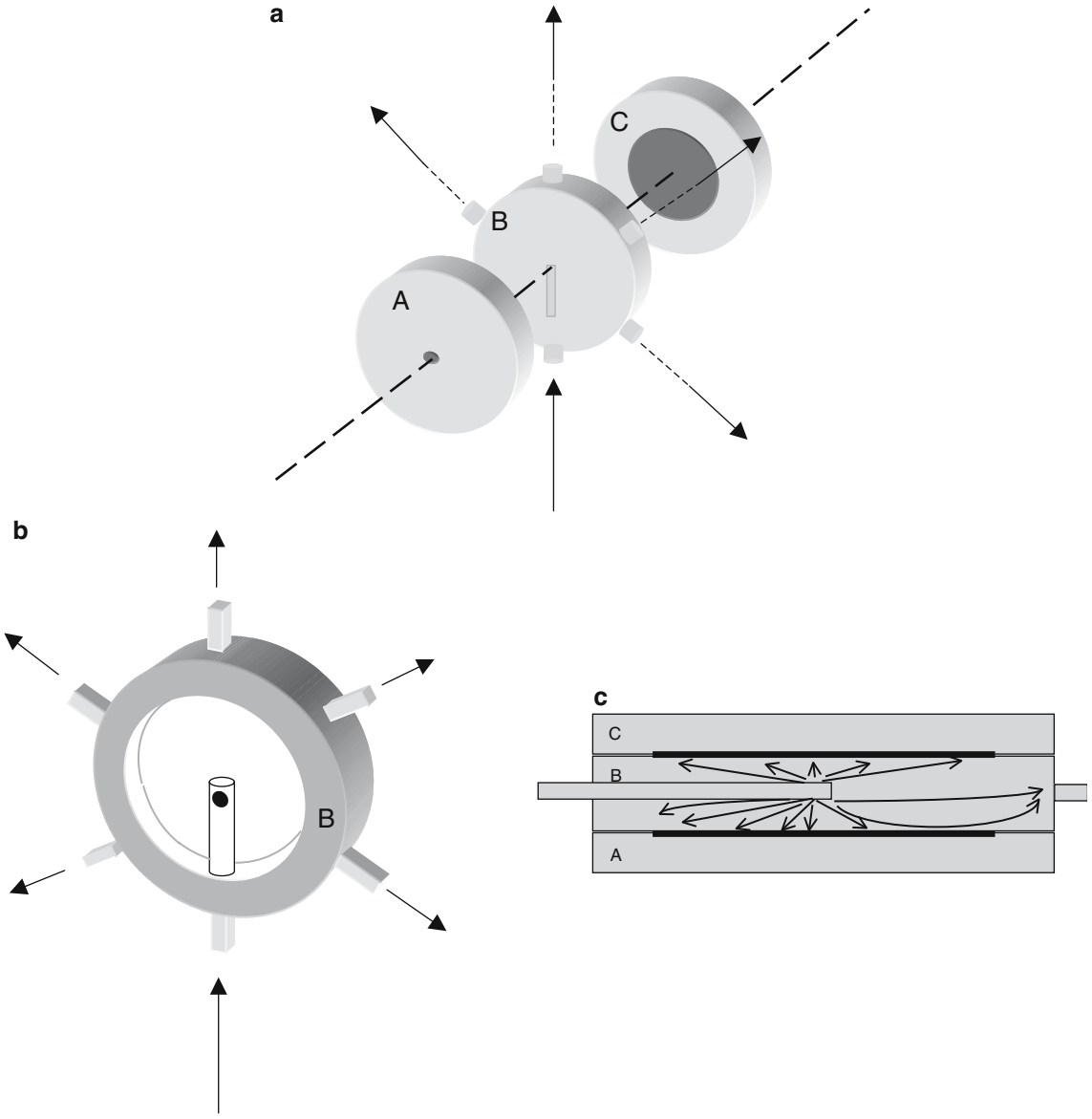

Fig. 1. Design of the electrochemical cell. (a) Different compartments of the cell: (A) anodic compartment, (B) electrolysis compartment and (C) Cathode compartment. (b) Electrolysis compartment: one inlet and several outlet sections. (c) Electrolyte distribution in the central compartment and towards electrode surfaces.

Fig. 2. View of the cell compartments, showing inlet and outlet connectors.

values, I_L, were obtained from curves at different redox couple concentrations, at different flow velocities). The mass transfer coefficient value was then obtained using:

$$K = \frac{1}{zFA} \times \frac{dI_L}{dC} \quad (1)$$

The impinging jet electrode configuration produces high local mass transfer rates [37]. The fluid dynamics

Table 1. Physical properties of the electrolyte, at 20 °C [4]

Density, ρ	1020.5	kg m^{-3}
Dynamic viscosity, μ	1.105×10^{-3}	kg m^{-1} s^{-1}
Kinematic viscosity, ν	1.083×10^{-6}	m^2 s^{-1}
Diffusivity of ferri-cyanide ion	6.631×10^{-10}	m^2 s^{-1}
Schmidt number, *Sc*	1633	–

and mass transfer characteristics of the impinging jet arrangement have been extensively studied [38–40]. As reported by Chin and Tsang, the dependence of mass transfer on fluid properties, hydrodynamics and cell geometry can be described through dimensional analysis, which leads to the following general expression [16]:

$$Sh = l \times Re^{m} \times Sc^{1/3} \quad (2)$$

where l and m depend on cell geometry. Considering the ratio between the radius of the electrode (R) and the diameter of the nozzle (d), Equation (2) is valid only for values of $R/d < 1$: under these conditions, the mass transfer coefficient (K) is independent of R. On the other hand, in the 'wall jet' region ($R/d > 1$), K depends on R and the same Equation (2) was used, leading to a mean value for K [16]. To evaluate the dimensionless numbers involved in Equation (2), the physical properties of ferro-cyanide solutions were used, the nozzle diameter d_N was used as the characteristic dimension, while the mass transfer coefficient values at different flow conditions were derived from Equation (1). The electro-oxidation of OA was then investigated in the same electrochemical flow cell, using a solution volume of 0.850 dm^3. Electrolyses were performed at room temperature (~ 25 °C), applying a constant current density of 100 A m^{-2}, with different anode materials (Ti/Pt, Si/BDD, Pb/PbO_2 and Ti/IrO_2–Ta_2O_5). A graphite cathode was used. The Pb/PbO_2 electrode was prepared by anodising a Pb disk plate in 10% M H_2SO_4, at 50 °C and 50 A m^{-2}, for 1 h [41]. Thin, highly boron-doped diamond (BDD) films were synthesized by Adamant Technologies (Neuchâtel, Switzerland). The BDD was grown onto a conductive p-Si substrate (0.1 Ω cm, Siltronix) via the hot-filament, chemical-vapour-deposition technique (HF-CVD) [42, 43]. This procedure gave a columnar, randomly textured, polycrystalline diamond coating, with a thickness of about 1 μm and a resistivity of 15 mΩ cm (± 30%). Both the Ti/Pt and Ti/IrO_2–Ta_2O_5 electrodes were kindly provided by De Nora (Milan, Italy).

Constant current experiments were performed with an Amel model 553 galvanostat. During the various electro-oxidation tests, the OA concentration was determined by means of a conventional titration method, using a 0.02 M $KMnO_4$ (Fluka) solution. Standardization was obtained by titration of a known amount of anhydrous and pure oxalic acid. Fresh 0.1 M solutions of OA (Fluka, dihydrate salt) were prepared in 0.5 M H_2SO_4 (Riedel-de-Haën) using distilled water.

3. Results and discussion

3.1. *Mass transfer coefficient*

Polarization curves are shown in Figure 3. The data were obtained at different ferro/ferri-cyanide concentrations (from 10 to 30 mM, in 0.5 M NaOH) and at a constant flow rate ($Q = 1.83\times10^{-5}$ m^3 s^{-1}). From these curves, the dependence of the limiting current on substrate concentration (Figure 4) and solution flow rate (Figure 3 inset) was determined. Figure 4 shows the expected linear dependence of the limiting current on the ferro-cyanide concentration. The mass transfer coefficient (K) has a value of 2.97×10^{-5} m s^{-1}. This represents a considerable improvement with respect to the value of 1.77×10^{-5} m s^{-1} obtained with a former design of the electrochemical cell (one peripheral inlet and only one outlet, diametrically opposed) [44]. The chosen flow rate ($Q = 1.83\times10^{-5}$ m^3 s^{-1}, which corresponds to 60% of the available pump power) used during the cell characterization provided the best OA oxidation trend, as shown in Figure 5.

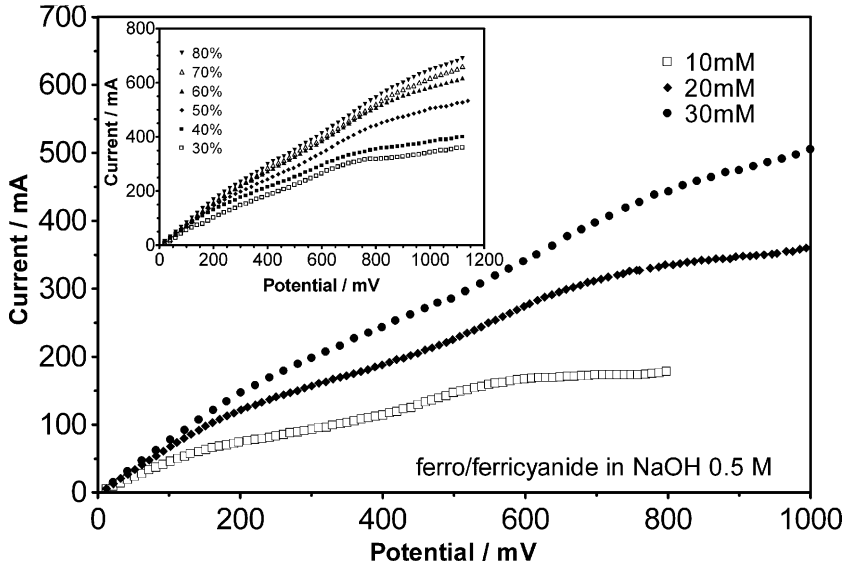

Fig. 3. Polarization curves for the engineering characterization of the electrochemical cell, using the ferro/ferri-cyanide redox couple. Inset: Determination of the limiting current at different flow rates (% of pump power) at 30 mM $Fe[CN]_6^{3-/4-}$, in 0.5 M NaOH.

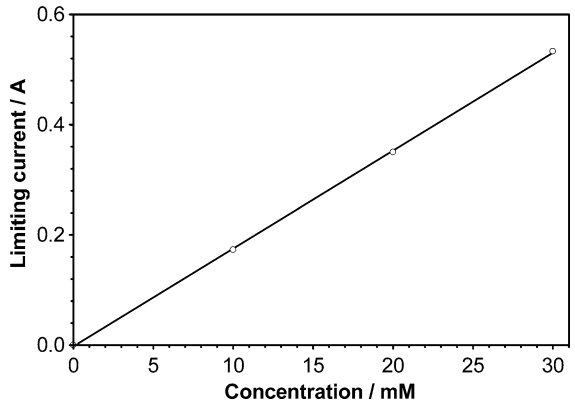

Fig. 4. Plot of limiting current vs. ferro-cyanide concentration.

In addition to the mass transfer coefficient increase, the new cell design allows better distribution of the electrolyte on the electrode surface. Making use of correlations obtained from dimensional analysis [45], the mass transfer coefficient was also determined theoretically. Data were correlated using the following dimensionless parameters:

$$Re_d = \frac{V_N d_N}{v}, \quad Re_r = \frac{V_N r}{v} \tag{3}$$

$$Sh_d = \frac{K_m d_N}{D}, \quad Sh_r = \frac{K_m r}{D} \tag{4}$$

$$Sc = \frac{v}{D} \tag{5}$$

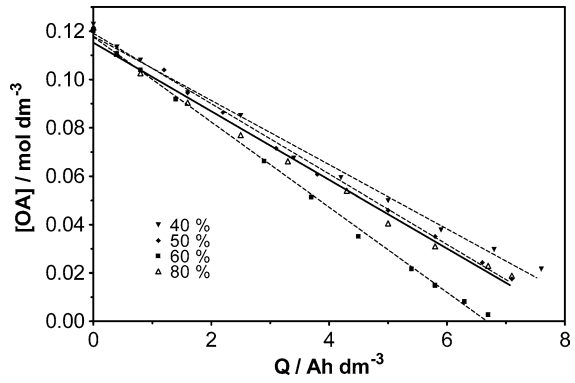

Fig. 5. Electro-oxidation of OA at the BDD electrode, at 100 A m^{-2} and at different flow rates, depending on pump power (see Table 2 for details).

where:

$$v = \frac{\mu}{\rho} \tag{6}$$

The parameters Sh_d and Re_d are used to describe effects in the impingement zone, while Sh_r and Re_r are used to describe effects in areas at a radial distance r from the impingement point. Data for the different flow conditions are reported in Table 2.

Data obtained from Equations (3) and (4) tally well with Equation (2), provided values of 0.89 and 1.1 are used for l and m, respectively. These values differ from those previously obtained for different cell geometries [16], in which the l value decreases with the ratio between the radius of the electrode and the nozzle diameter, while the m value increases with R/d up to an asymptotic value. Such divergence may be due to differences between the single outlet in the conventional impinging jet cell and the existence of several outlets in the present cell.

The mass transfer coefficient for this electrochemical cell can be thus estimated: for an electrolyte flow of 1.83×10^{-5} m^3 s^{-1}, Sh_r and Re_r values of 119 and 2138 are obtained (Equations (3) and (4)); the K value, calculated using Equation (2) and considering the values obtained for m and l, is 2.99×10^{-5} m s^{-1}. Interestingly, the experimentally determined value of K is practically equal to the value thus obtained.

3.2. *Anodic oxidation of oxalic acid*

3.2.1. *Oxalic acid oxidation and kinetics*

The anodic oxidation of OA was carried out at a constant temperature (25 °C) and at a current density J of 100 A m^{-2}. The process was studied at Si/BDD, Pb/PbO_2, Ti/Pt and Ti/IrO_2–Ta_2O_5 electrodes.

The results obtained at the BDD electrode, at different flow rates, are shown in Figure 5. The fastest incineration of the organic substrate was realized at an electrolytic flow rate of 1.83×10^{-5} m^3 s^{-1}, for which the mass transfer coefficient was 2.97×10^{-5} m s^{-1}. Faster pumping rates induce a decrease in the substrate oxidation rate, as shown by the results obtained with a flow rate of 2.53×10^{-5} m s^{-1} (80% of the pump power). Figure 6 shows that OA oxidation can be obtained with a charge consumption of 7 Ah dm^{-3}, i.e., with a 90% total faradic yield. The total incineration of OA requires a theoretical charge consumption of 6.3 Ah dm^{-3}. Whilst a comparison with results obtained in a

Table 2. Hydrodynamic parameters for the new cell design

Pump power %	20	30	40	50	60	70	80	90
Flow m^3 s^{-1} $\times10^{-6}$	4.16	7.66	11.2	14.7	18.3	21.8	25.3	28.0
Re_d	2.72	5.01	7.33	9.63	11.98	14.28	16.37	18.34
Re_r	27.25	50.18	73.37	96.30	119.88	142.81	163.78	183.43
Sh_d	117.96	131.97	142.58	186.03	213.81	224.87	242.19	252.15
Sh_r	1179.63	1319.71	1425.84	1860.35	2138.08	2248.67	2421.92	2521.46
K m $s^{-1}\times10^{-5}$	1.73	1.94	2.10	2.74	3.15	3.31	3.56	3.71

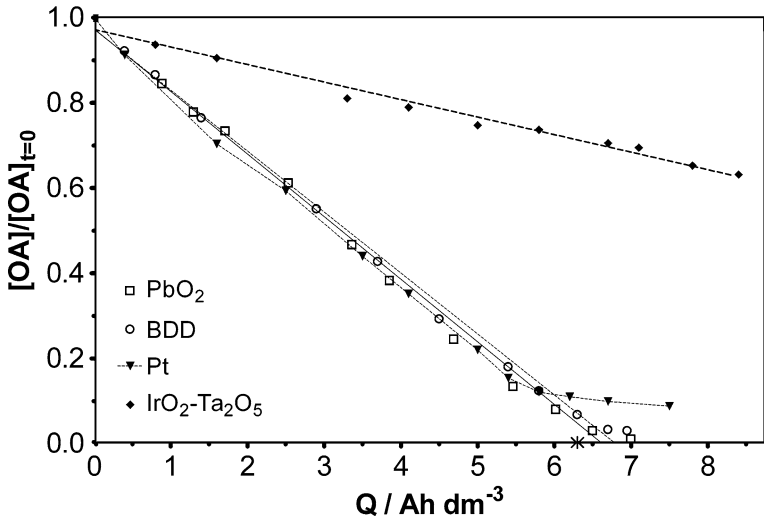

Fig. 6. Comparison of OA elimination at Pt, PbO_2, BDD and IrO_2–Ta_2O_5 electrodes. Data obtained at 100 A m^{-2}, [OA] = 0.12 M, flow rate = 1.83×10^{-5} m^3 s^{-1} and 25 °C. The asterisk in the X-axis represents the theoretical specific charge required for total OA incineration.

batch-type cell [46] is not strictly possible (because of the different composition and preparation path of the diamond electrode used), the improvement in faradic yield attained with the flow-cell (especially in the final stages of the process) can be ascribed to a more effective mass transport.

The anodic oxidation of OA was also carried out at a Ti/Pt electrode under the same conditions applied for the BDD electrode. With regards to the results collected in Figure 6, the main features of the oxidation process do not differ significantly from those with BDD. As already observed in [46], the anodic oxidation process initially exhibits a faradic yield close to 100%, which gradually decreases to zero in the final stages of the process. This evidence further supports the hypothesis that when low concentrations of organic depolariser are attained, the role of the concomitant oxygen evolution becomes decisive. This increases the efficiency of the parasitic reaction (experiments are carried out at constant J) causing changes at the Pt electrode surface, which decreases its activity towards the OA oxidation, favouring the concomitant oxygen evolution.

Again in good agreement with the measurements carried out in batch reactor, the faradic efficiency of the OA oxidation at the Pb/PbO_2 electrode is very high, practically 100% down to very low residual substrate concentrations (Figure 6). Both these results and the ones at BDD and Ti/Pt were obtained at electrode materials not identical to those used in [46], differing in terms of preparation, in the detail of their surface texture and, to a certain extent, also in their composition and microstructure (in the case of Pb/PbO_2). On the other hand, the anodic oxidation/incineration of OA seems to take place with efficiency close to 100% at electrode materials with quite different properties. Again, at Pt electrodes undergoing thicker oxide film formation (at high anodic polarizations), the oxygen evolution reaction becomes favoured, practically excluding oxidative attack on the organic substrate. In all likelihood, the nature of Pt oxide films formed at high anodic polarization exhibits much poorer adsorptive properties toward the OA molecule, water oxidation consequently becoming the kinetically favoured process. Analogous reasons may be proposed for the trend of the OA anodic oxidation at Ti/IrO_2–Ta_2O_5 electrode, also shown in Figure 6. In this case, however, the insufficient activity of the electrode material is evident from the very beginning of the galvanostatic experiment, reflecting structural and catalytic properties of the oxide film already achieved by the preparation procedure, rather than through modifications undergone by the electrode during the electrochemical experiment. Apparently, in the case of thermally (IrO_2) or anodically-prepared (Pt) group VIII noble-metal oxides, the nature and reactivity of active sites favour interaction with water molecules and hydroxyl radicals which, displacing the OA species, makes its oxidation extremely slow.

4. Conclusions

The proposed flow-cell guarantees effective and reproducible mass transport. The inter-electrode space is properly exploited and the cell geometry and flow direction, from the centre toward the periphery, ensures a progressive lowering of the solution flow rate while the reactant is consumed. Some problems encountered at higher flow-rates highlight the need for further improvement in cell design.

The results on oxalic acid oxidation at Si/BDD, Ti/Pt, Pb/PbO_2 and Ti/IrO_2–Ta_2O_5 electrodes, under controlled mass-transport conditions, support the hypothesis formulated in [46] that the reaction is conditioned by a fast adsorption stage. It is confirmed, in particular, that the anomalous decrease in the process rate at Pt electrodes, when the substrate concentration decreases below certain critical values, can be related to changes in the electrode surface at higher anodic potentials as a

consequence of the lack of organic depolarisers [46]. These changes seem to generate active sites at the PtO_x surface which are no longer suitable for OA adsorption, thus resembling the case of a IrO_2–Ta_2O_5 electrode, typically a very good catalyst for the oxygen evolution reaction.

Acknowledgements

C.A. Martinez-Huitle gratefully acknowledges the CONACYT for financial support of his Ph.D. The authors thank Adamant Technologies (Neuchâtel, Switzerland), for providing the BDD samples, and De Nora (Milan, Italy) for the Ti/Pt and Ti/IrO_2–Ta_2O_5 electrodes.

References

1. C.F. Oduoza and A.A. Wragg, *J. Appl. Electrochem.* **30** (2000) 1439.
2. W.N. Taama, R.E. Plimley and K. Scott, 'Mass transfer rates in a DEM electrochemical cell', proceedings of the 4th European Symposium on Electrochemical Engineering (CHISA), Institute of Chemical Technology, Prague (1996) pp. 289–295.
3. F. Goodridge, G.M. Mamoor and R.E. Plimley, *IChemE Symp. Ser.* **98** (1985) 61.
4. A.A. Wragg and A. Leontaritis, *Chem. Eng. J.* **66** (1997) 1.
5. A.A. Wragg, D.J. Tagg and M.A. Patrick, *J. Appl. Electrochem.* **10** (1980) 43.
6. C. Bengoa, A. Montillet, P. Legentilhomme and J. Legrand, *J. Appl. Electrochem.* **27** (1997) 1313.
7. C.F. Oduoza and A.A. Wragg, *Chem. Eng. J.* **85** (2002) 119.
8. L.H. Mustoe and A.A. Wragg, *J. Chem. Tech. Biotechnol.* **31** (1981) 317.
9. L.H. Mustoe and A.A. Wragg, *J. Appl. Electrochem.* **13** (1983) 507.
10. A. Djati, M. Brahimi, J. Legrand and B. Saidani, *J. Appl. Electrochem.* **31** (2001) 833.
11. C.F. Oduoza and A.A. Wragg, *Chem. Eng. J.* **68** (1997) 145.
12. A.A. Wragg and A. Leontaritis, *Dechema Monographs* **123** (1991) 345.
13. A.M. Polcaro, A. Vacca, S. Palmas and M. Mascia, *J. Appl. Electrochem.* **33** (2003) 885.
14. K. Jüttner, U. Galla and H. Schmieder, *Electrochim. Acta.* **45** (2000) 2575.
15. S. Yapici, S. Kuslu, C. Ozmetin, H. Ersahan and T. Pekdemir, *J. Appl. Electrochem.* **29** (1999) 185.
16. D.-T. Chin and C.-H. Tsang, *J. Electrochem. Soc.* **125** (1978) 1461.
17. H. Martin, *in* J.P. Hartnett and T.F. Irvine, Jr. (Eds), 'Advances in Heat Transfer', Vol. 13, (Academic Press, New York, 1977), pp. 1–60.
18. F.P. Incropera and D.P. de Witt, *Fundamentals of Heat and Mass Transfer*, 3rd ed., (John Wiley & Sons, New York, 1990), p. 431.
19. D. Gandini, E. Mahè, P.A. Michaud, W. Haenni, A. Perret and Ch. Comninellis, *J. Appl. Electrochem.* **30** (2000) 1345.
20. Ch. Comninellis and E. Plattner, *Chimia* **42** (1988) 250.
21. Ch. Comninellis and C. Pulgarin, *J. Appl. Electrochem.* **21** (1991) 703.
22. Ch. Comninellis, *Gas Wasser, Abwasser.* **11** (1992) 792.
23. Ch. Comninellis and C. Pulgarin, *J. Appl. Electrochem.* **23** (1993) 108.
24. Ch. Comninellis, E. Plattner, C. Seignez, C. Pulgarin and P. Péringer, *Swiss Chem.* **14** (1992) 25.
25. C. Pulgarin, N. Alder, P. Péringer and Ch. Comninellis, *Water Res.* **28** (1994) 887.
26. A.M. Polcaro, M. Mascia, S. Palmas and A. Vacca, *Ind. Eng. Chem. Res.* **41** (2002) 2874.
27. Comninellis Ch., *Electrochim. Acta* **39** (1994) 1857.
28. A.M. Polcaro, S. Palmas, F. Renoldi and M. Mascia, *J. Appl. Electrochem.* **29** (1999) 147.
29. N. Belhadj Tahar and A. Savall, *J. Electrochem. Soc.* **145** (1998) 3427.
30. J. Feng, L.L. Houk, D.C. Johnson, S.N. Lowery and J.J. Carey, *J. Electrochem. Soc.* **142** (1995) 3626.
31. F. Bonfatti, S. Ferro, F. Lavezzo, M. Malacarne, G. Lodi and A. De Battisti, *J. Electrochem. Soc.* **146** (1999) 2175.
32. G. Foty, D. Gandini and Ch. Comninellis, *Current Top. Electrochem.* **5** (1997) 71.
33. Ch. Comninellis and A. De Battisti, *J. Chim. Phys.* **93** (1996) 673.
34. V. Fisher, D. Gandini, S. Laufer, E. Blank and Ch. Comninellis, *Electrochim. Acta* **44** (1998) 521.
35. M. Fryda, D. Herrmann, L. Schafer, C.-P. Klages, A. Perrer, W. Haenni, Ch. Comninellis and D. Gandini, *New Diamond Front. Carbon Technol.* **9** (1999) 229.
36. D.J. Tagg, M.A. Patrick and A.A. Wragg, *Trans. I. Chem. Eng.* **57** (1979) 176.
37. Y.M. Chen, W.T. Lee and S.J. Wu, *Heat Mass Transfer* **34** (1998) 195.
38. C.J. Chia, F. Giralt and O. Trass, *Ind. Eng. Chem. Fundam.* **16** (1977) 28.
39. F. Giralt and O. Trass, *Can. J. Chem. Eng.* **53** (1975) 505.
40. M.T. Scholtz and O. Trass, *AIChE J.* **16** (1970) 82.
41. W. Fresenius, Water Analysis. Ed. Springer-Verlag, Berlin Heidelberg Germany, (1998) p. 477.
42. S. Ferro, *J. Mater. Chem.* **12** (2002) 2843.
43. A. Perret, N. Skinner, Ch. Comninellis and D. Gandini, *Electrochem. Soc. Proc.* **32** (1997) 275.
44. Michaud P.A., PhD Thesis No. 2595 (2002) EPFL-Switzerland.
45. Zin G.K., U.S Patent 3,196,832 (1965).
46. C.A. Martinez-Huitle, S. Ferro and A. De Battisti, *Electrochim. Acta* **49** (2004) 4027.